Experimental investigation of ignition temperatures of aluminum particles

Fabien Halter, Valentin Glasziou, Hugo Keck, Guillaume Legros, Christian Chauveau

13th U. S. National Combustion Meeting
Organized by the Central States Section of the Combustion Institute
March 19–22, 2022
College Station, Texas

Experimental investigation of ignition temperatures of aluminum particles

F. Halter[1], V. Glasziou[1,3], H. Keck[2], G. Legros[1], C. Chauveau[2]

[1]*ICARE- CNRS, Université d'Orléans, 1C Avenue de la Recherche Scientifique, Orléans, France*
[2]*ICARE- CNRS, 1C Avenue de la Recherche Scientifique, Orléans, France*
[3] *CEA Centre Gramat*
[*]*Corresponding Author Email: fabien.halter@cnrs-orleans.fr*

Abstract:
Aluminum particles are widely used as an additive to increase energetic performances. Recently, Aluminum has also received a growing interest as a source of hydrogen for fuel cell applications, or in novel power generation concepts as it provides a carbon-free energy that meets current policies for reducing emissions of greenhouse gases. Our recent studies focused on the description of the combustion process varying ambient conditions (pressure and oxidizer). Only the second stage of the combustion process, after the establishment of a steady state, was scrutinized. The proposed work sheds light more specifically to the initial stages where the particle is warmed up from the initial state to a thermal runaway condition. Indeed, the question arises at what temperature do these condensed fuels burst into flames, knowing that the presence of a passive coat greatly influences the process.

For this study, a dedicated set-up has been improved. It consists of an electrodynamic levitator in which a single particle, trapped by electrostatic forces, burns in a controlled atmosphere. A two-color ratio pyrometer has been specifically assembled with photomultipliers (PM) to obtain the time evolution of mean surface temperature. The PM signals are synchronised witha particle visualization device that is composed of a high-speed camera combined with a long-distance microscope. Subsequently, the temperature measurement of high temporal resolution can then be associated for the first time at a rate of 250 000 fps with the fast-apparent phenomenology of the pre-ignition processes. In addition, the spatial resolution of the visualization (1.92 μm/pix) allows the interpretation of the PM signals to be commented.

Keywords: Metal fuels, Aluminum particle, ignition temperature

1. Introduction

Knowledge about the specific ignition temperature is crucial to the accurate modelling of the performances of practical combustion systems using metal particles such as propulsion systems, explosives, and pyrotechnics. Yet efforts to characterize aluminum ignition have produced up to now results that are contradictory. A major difficulty comes from the presence of the passive natural oxide that covers the particle. This coating consists of a thin layer of amorphous alumina whose thickness has been

evaluated to vary from about 0.5 nm to 4 nm. Most of the authors suggest that micrometric aluminum powders are coated with a 2 – 3 nm thick layer [1-4].

Friedman and Macek [5] speculated that ignition of aluminum occurs upon melting of the oxide film, leading to an ignition temperature of Al close to the melting point of Al_2O_3 (i.e., 2345 K). However, ignition temperatures as low as 850 K and as high as 2400 K have been reported [9-19]. The reported range of temperature appears to correlate with the mean particle diameter [20]. The observed discrepancies may also be attributed to different experimental methods employed, which resulted in different conditions, such as surrounding gas compositions and heating rates. The main experimental techniques illustrating the different heating regimes leading to aluminum ignition are the Thermal Analysis [3], the Wire Ignition [6], the Shock Tube [7], and the laser heating [8]. The kinetics of exothermic reactions is commonly characterized by thermal analysis, where heating rates are very low (lower than 10^1 K/s) in comparison with heating rates of practical interest (higher than 10^5 K/s), which are not readily controlled. For the simplest analysis of a metal particle ignition in a practical combustion system, the rate of particle heating by external sources as it enters the combustion system should be compared against the thermal losses and the rate of particle self-heating due to oxidation. This study, based on both detailed experiments and a simplified thermal model, brings new insights into the ignition sequence and addresses the relative importance of the phenomena at play.

2. Experimental set-up description

The experimental device is mainly composed of a high-pressure combustion chamber into which an electrostatic levitation system is incorporated. The particle, initially charged with triboelectric effect, is introduced in the electric field in the center of the levitator. Electric forces generated by the levitator allow the charged particle to remain motionless at the center of the chamber without any contact with any surface. The temperature increase of the particle due to the laser heating leads to thermionic losses. In the case of aluminum with a work function that ranges between 4 and 4.2 eV, the characteristic time for charge loss is shown to be around 1 ms at 1300K [9].

This single particle is isolated in the center of the chamber by modulating the different voltages of the levitator. A CO_2 laser (power of 50 W, wavelength of 10.6 µm) is used to warm up the particle till ignition. Once the combustion is initiated, the laser is stopped. The particle stabilized in levitation is heated almost uniformly on both sides as the initial beam is carefully splitted into 2 ones of equivalent power. Opposed laser beams are focused in the center of the chamber leading to an estimated beam waist $D_{beam} = 193\ \mu m$ at the particle's location. The positioning of the particle relative to the laser beam will be discussed later (see Section 3). The high-pressure chamber (up to 12 MPa by design) allows combustion experiments to be conducted in a controlled gaseous atmosphere, and with a wide variety of gas composition. Particles with diameters ranging from 20 to 150 µm can be stabilized with this system.

The time evolution tracking of the burning particle is ensured by the use of an imaging device combining a fast camera PHANTOM and a long-distance microscope QUESTAR QM100 focused on the particle in reaction. The camera used is the PHANTOM V2512, allowing 25000 fps at maximum resolution (1280x800 px) up to 39000 fps at the resolution used in this study (768x768 px). The magnification obtained with the long-distance microscope is 1.92 µm/px. The imaging obtained by the fast camera allows not only a phenomenological description of the combustion process, but also, after the application of an image processing, the extraction of quantitative information such as for example the diameter of the initial aluminum particle after melting, the temporal evolution of this diameter, the migration speed of the alumina particles towards the drop, etc.

The method selected to measure experimentally the temperature is the 2-color pyrometry. This method makes it possible to determine the temporal evolution of the average temperature of the condensed phase during the combustion of the aluminum particle [10-12]. To achieve this, an optical system composed of 2 photomultipliers (Thorlabs PMT1002) is set up to follow the temporal evolution of the light signal emitted by the particle during its combustion. The PMTs are operating in a spectral range between 250 and 900 nm and at a frequency of 250 kHz. A USB-1808X acquisition card is used to digitize the signal. Each PMT is equipped with an interference filter (λ_1=720 nm and λ_2=830 nm with a 10nm FWHM). This couple of spectral ranges has been selected to avoid the emission lines of the major gaseous species identified by the literature in the reaction zone. As a result, the signal captured by the PMs is supposed to be highly dominated by the emission of the condensed matter's surface.

A schematic view of the full set-up is proposed in Figure 1.

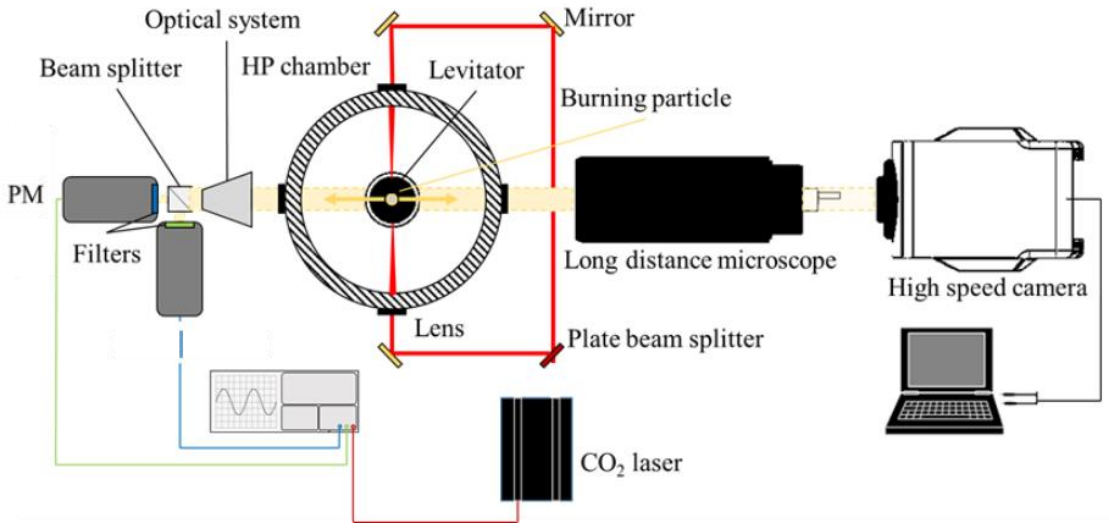

Figure 1 : Schematic view of the complete experimental set-up

The pyrometer is calibrated using a certificated 45 W Quartz Tungsten Halogen Lamp (Newport). We assume in the following that the emissivity of the condensed matter does not vary over the selected spectral range (i.e. 720 nm to 830 nm) which is consistent in view of our latest results [13].

Evaluating the ratio of the radiative intensity, $\Gamma = L_{\lambda_1}/L_{\lambda_2}$, as given by Planck's law and measured over both selected spectral rangesthe expression for the temperature is derived as follows:

$$T\,(\Gamma,\lambda_1,\lambda_2) = \left[\frac{k}{h.c}\,.\frac{\lambda_1.\lambda_2}{\lambda_2-\lambda_1}.\left(ln(\Gamma)\;-\;5.ln\left(\frac{\lambda_1}{\lambda_2}\right)\right)\right]^{-1} \qquad \textit{Equation 1}$$

with k the Boltzmann constant, h the Planck constant, and c the speed of light in vaccuum.

A major assumption of the processing is that the signal's absorption along the line-of-sight leading to the PM's is neglected. Actually, this assumption may lead to significant uncertainties in the evaluation of the radiative heat feedback from the flame to the condensed matter [14]. Still, the assumption skews at a similar level both signals as they are collected over close spectral ranges and the interpretation of their ratio delivers decent evaluation of the surface's temperature [15].

More details about this device are given in Ref. [16].

3. Model description

The system we consider for this model is composed of an aluminum particle, covered with a thin layer of alumina and located in an oxidizing medium. The model is constructed to describe the average temperature of the particle surface until its ignition. In the case of our experimental setup, the particle's diameter is typically of the order of 20-100 μm, and the combustion process happens at the latest 10 ms after the start of the heating process. As a first approximation, the ignition temperature in this model is considered to be the alumina melting temperature $T_{melt\_Al_2O_3} = 2345\,K$. Within the range of the particle's size studied, heat conduction in the particle dominates the convective exchanges occurring at the surface, leading to a Biot number << 1. Consequently, we consider in the sequel that the temperature gradients are negligible throughout the particles.

As described in the experimental section, the particle is heated until its ignition with a 50 W CO_2 laser (λ =10.6 μm). An optical efficiency, due to the different optics met along the optical pathways (i.e. mirrors, windows, and lenses) has been experimentally evaluated to be 0.84. Thus, a power of 42 W distributed along a gaussian profile is considered to be delivered by the laser at the center of the combustion chamber. The experimental setup allows a symmetrical heating of the particle by the careful splitting of the laser illuminating the particle from both sides. However, for the sake of clarity, a single laser beam is considered in this model. Thermal losses by conduction and radiation towards the surroundings are considered while convection is neglected as the particle is considered spatially static and because of the absence of any flow induced within the very short process studied.

The numerical model is a sequence of three phases. The first one consists in the heating of the particle from room temperature to the melting point of aluminum. During this phase, the energy transmitted from the laser to the particle is used to heat up the particle up to 933 K. When this temperature is reached, the energy from the laser is mainly used to melt the aluminum, that the second phase of the model characterizes. This phase is assumed to take place at constant temperature. When the aluminum is fully melt, the last phase brings the temperature of the particle to its ignition temperature.

The heat delivered by the laser to the particle consists in the integration of the laser power density along the effective surface of the particle, weighed by its absorption efficiency η_{abs}. Little information is available in the literature on the absorption efficiency and even less on its evolution with the diameter and the temperature of the particle. For this model, we relied on the work of Mohan [17] as discussed later.

The power density of the laser being distributed along a gaussian profile, it can be expressed as follows:

$$I(y,z) = \frac{W}{2\,\pi\,\sigma^2}\, e^{\frac{-y^2}{2\,\sigma^2}}\, e^{\frac{-z^2}{2\,\sigma^2}} \qquad \textit{Equation 2}$$

W is the total power delivered by the laser (i.e. 42 W), σ is the standard deviation along the gaussian profile and as described by Mohan [17], it can be assumed that $6\,\sigma = D_{beam}$, where $D_{beam} = 193\,\mu m$. In other words, it can be considered that 99.7% of the power lies within the beam diameter D_{beam}. y and z are the coordinates from the center of the gaussian profile as indicated in Figure 2. The total power transmitted to the particle from the laser is then

$$\dot{Q}_{laser} = \eta_{abs} \int_{z_p-r_p}^{z_p+r_p} \int_{-\left(r_p{}^2-(z-z_p)^2\right)^{0.5}}^{z_p+r_p} I(y,z)\,dy\,dz \qquad \textit{Equation 3}$$

It is considered in this expression that the particle is centered along the y axis with respect to the gaussian profile, and shifted from the center of the gaussian profile along the z axis by z_p. The power density is integrated along the surface of a circle of radius r_p, that is the radius of the particle. Indeed, the effective surface illuminated from one side by the laser is $\pi\ {r_p}^2$. The laser lasts till the particle ignition following a top-hat function of time.

The absorption efficiency allows to quantify the amount of energy transmitted to the particle as an important part of the energy is reflected. This coefficient is theoretically derived in Ref. [18] and numerical values are given for aluminum in Ref. [17]. This coefficient depends on the temperature, the size of the particle (considered constant during the heating process), the refractive index of the material (alumina in our case), and the wavelength of the laser. The numerical values chosen for the model come from Ref. [17]. We consider the absorption efficiency to vary linearly from 0.018 to 0.08 between 300 and 2345K. The position of the particle with respect to the laser profile is represented in Figure 2. The particle is indicated by the grey circle. For simplicity, it is assumed to be spherical. The laser profile is represented by the blue Gaussian function. The particle position is vertically shifted by z_p with respect to the maximum of the Gaussian profile. No shift is considered in the y direction (note that the laser beam profile is assumed to be asymmetrical).

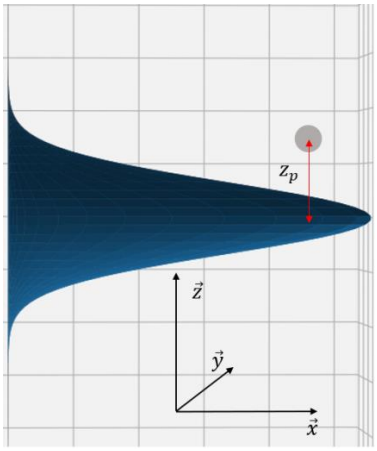

Figure 2 : View of the position of the particle (grey sphere) with respect to the laser profile (blue shaded region)

Once the laser power transferred to the particle is determined, the power used to heat the particle and the heat losses may be evaluated.

The heat to raise the temperature of the particle up to its melting point is

$$\dot{Q}_{heat} = m_p c_p \frac{dT}{dt} \qquad \textit{Equation 4}$$

m_p being the mass of the particle, c_p the heat capacity of aluminium, and T the temperature of the particle. The heat lost by radiation to the surrounding follows the Stefan-Boltzmann's law and is expressed as

$$\dot{Q}_{rad} = \sigma_{SB} \epsilon_{Al_2O_3} (T^4 - T_0^4) \qquad \textit{Equation 5}$$

With σ_{SB} the Stephan-Boltzmann constant, $\epsilon_{Al_2O_3}$ the emissivity of alumina as it is what the external layer of the particle is made of, and T_0 the room temperature. Then, heat losses by conduction through the particle's surface S_{part} follow the Fourier's law and can be expressed as

$$\dot{Q}_{diff} = -\lambda\, S_{part}\, \nabla T \qquad \textit{Equation 6}$$

λ being the thermal conductivity of the ambient gases. Expressing this term in spherical geometry, we get

$$\dot{Q}_{cond} = -\lambda\, 4\pi r^2\, \frac{dT}{dr} \qquad \textit{Equation 7}$$

Then, integrating between the particle radius and an infinite distance

$$\dot{Q}_{cond} = -\lambda\, 4\pi r_p (T - T_0) \qquad \textit{Equation 8}$$

For a particle temperature below the melting temperature of aluminum, we can thus write

$$\dot{Q}_{laser} = \dot{Q}_{heat} + \dot{Q}_{rad} + \dot{Q}_{cond} \qquad \textit{Equation 9}$$

When reaching the melting point of aluminum, the energy transmitted to the particle is used for melting at constant temperature $(T_{melt\_Al} = 933\ K)$.

$$\dot{Q}_{melting} = L_{Al}\, \frac{d\, m_{liq\_Al}}{dt} \qquad \textit{Equation 10}$$

With L_{Al} the latent heat of fusion and m_{liq_Al} the mass of liquid aluminum. Thus, at the melting temperature of aluminum and while the aluminum is not fully molten, we write

$$\dot{Q}_{laser} = \dot{Q}_{melting} + \dot{Q}_{rad} + \dot{Q}_{cond} \qquad \textit{Equation 11}$$

Once the aluminum only exists in its liquid phase and up to the ignition temperature, we use Eq. 11.

We thus have a system of equation that we can solve with respect to the temperature

$$\begin{cases} \dot{Q}_{laser} = \dot{Q}_{heat} + \dot{Q}_{rad} + \dot{Q}_{cond} & when \quad T_{particule} < 933\ K \\ \dot{Q}_{laser} = \dot{Q}_{melting} + \dot{Q}_{rad} + \dot{Q}_{cond} & when \quad T_{particule} = 933\ K \\ \dot{Q}_{laser} = \dot{Q}_{heat} + \dot{Q}_{rad} + \dot{Q}_{cond} & when \quad T_{particule} > 933\ K \end{cases} \qquad \textit{Equation 12}$$

In this way, it is possible for a given particle radius and particle height above the peak of the laser gaussian profile z_p to compute the temperature of the particle with respect to time and the contribution of each term (laser and losses) to the particle.

In the proposed model, the heat produced by surface reaction on the particle has been neglected as it is supposed that the thermal runaway occurs as soon as the oxide layer breaks. This hypothesis will be confirmed later.

4. Ignition process description

An aluminum particle is isolated and stabilized in the center of the levitator. The particles studied here have a size between 30 and 100 µm. The surrounding gas is composed of air at atmospheric conditions.

Figure 3 displays the ignition process of an aluminium particle having an initial diameter of 88 µm. The initial morphology of the particle is not exactly spherical as seen in the early stages of the process ($t1$ to $t4$). When subjected to CO_2 laser heating, we observe an increase in particle luminosity due to an increase in temperature. Unfortunately, the sensitivity of the camera and the selected exposure time (i.e. 10 µs) do not allow to detect the particle before the initial time $t1 = 2450\ \mu s$ of the sequence captured. Till $t4 = 3116\ \mu s$, the morphology of the particle remains almost unchanged. Only slight modifications can be observed on smallest structures. These changes are hardly discernible with the current image display quality. More or less luminous zones are observed on the surface of the particle. These differences can be linked to the presence of an non-uniform oxide layer thickness on the surface or to non-uniform

heating. As a reminder, the particle has an equivalent diameter of 88 µm while the diameter of the laser beam waist is approximately of 200 µm. In addition, the particle is simultaneously heated from both sides. However, it cannot be ruled out that the powers of the two laser beams are not perfectly balanced.
At $t5 = 3142\ \mu s$, the particle becomes spherical. It is still covered with alumina but the latter must have changed phase exposing, in certain areas, bare liquid aluminum to the surrounding oxidizer.
The evaporation of the liquid aluminum is no longer hindered by the presence of the oxide layer. An increase in luminosity is observed in the close vicinity of the drop. Vaporized aluminum reacts extremely fast with the oxygen of air to produce alumina. Since the local temperature is lower than alumina dissociation temperature (as confirmed later), alumina instantly condenses in the form of nanoparticles. These nanoparticles are at very high temperature (~3500 K) and emit radiation. Thermal runaway is clearly observed as soon as the oxide layer breaks. Observations clearly indicate that for these heating rates, heterogenous reactions on the liquid aluminum surface play a very limited (if not zero) role in the ignition processes.
After $t5 = 3142\ \mu s$, the alumina recovering the surface retracts to form several lobes which eventually merge into a single one. This process lasts around $600\ \mu s$ from $t6 = 3168\ \mu s$ till $t10 = 3783\ \mu s$. The laser is stopped after $t_{LASER} = 3600\ \mu s$, i.e. between $t9$ and $t10$. The energy provided by the laser after the thermal runaway induces an over-production of aluminum vapour, which accelerates the process to reach steady state. As soon as the laser is stopped, the dimension of the luminous halo (corresponding to the gas phase reaction zone) remains unchanged. Thermal equilibrium is reached almost immediately. Subsequently, the combustion of the aluminum drop continues following approximately a d^2-law [19, 20].

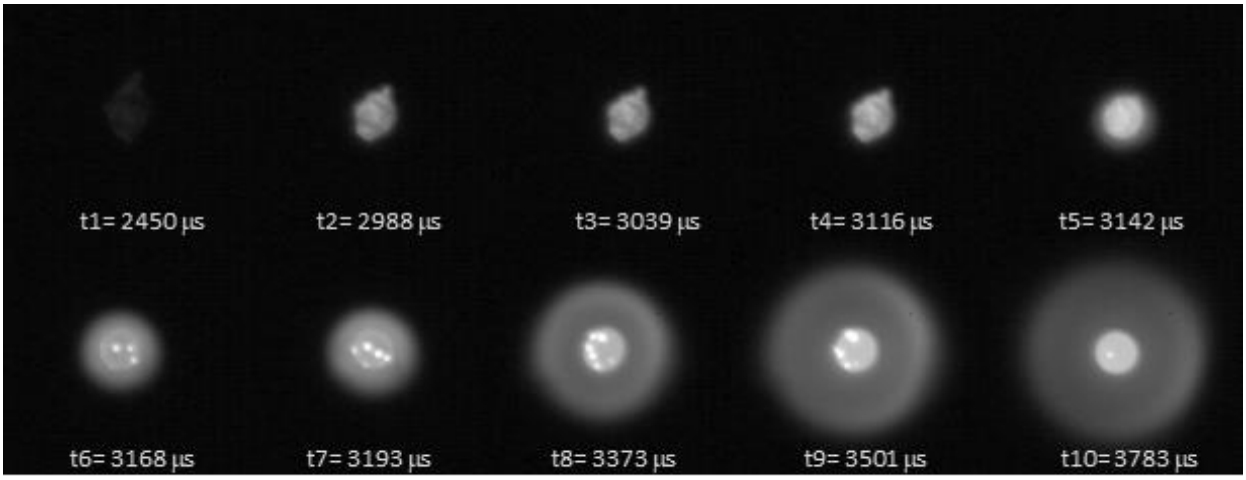

Figure 3 : Sequence of frames captured by the high-speed camera within the heating and ignition processes of an aluminium particle (initial diameter: 88 µm).

5. Temperature evolution during the ignition process

In this part, we compare the temperature evolution obtained with that measured experimentally. First, the relative contributions of the different terms involved in the energy equation (Eq. 13) (i.e. Q_{heat}, Q_{rad}, Q_{diff}) are evaluated. The total laser power (P_{LASER}) is taken constant and equal to 42 W. The vertical shift (z_p) is adjusted to 42 µm. This value was calibrated by positioning the particle relative to the laser by adjusting the settings of the levitator (i.e. modulating the different voltages of the levitator).
Figure 4 is limited to the first 3 ms after the start of the laser shot. The power transmitted by the laser to the particle (solid black line) is not constant, due to a variable absorption efficiency with the particle temperature. We clearly identify three successive phases corresponding to: i) heating of solid aluminum

(till 1.2 ms) ii) aluminium fusion (till 1.7 ms) iii) heating of liquid aluminum (till the end). Over the entire heating, the power provided by the laser is much higher (at least two orders of magnitude) than losses by diffusion (solid red line) and radiation (solid blue line). We can therefore consider that the ignition process is almost adiabatic.

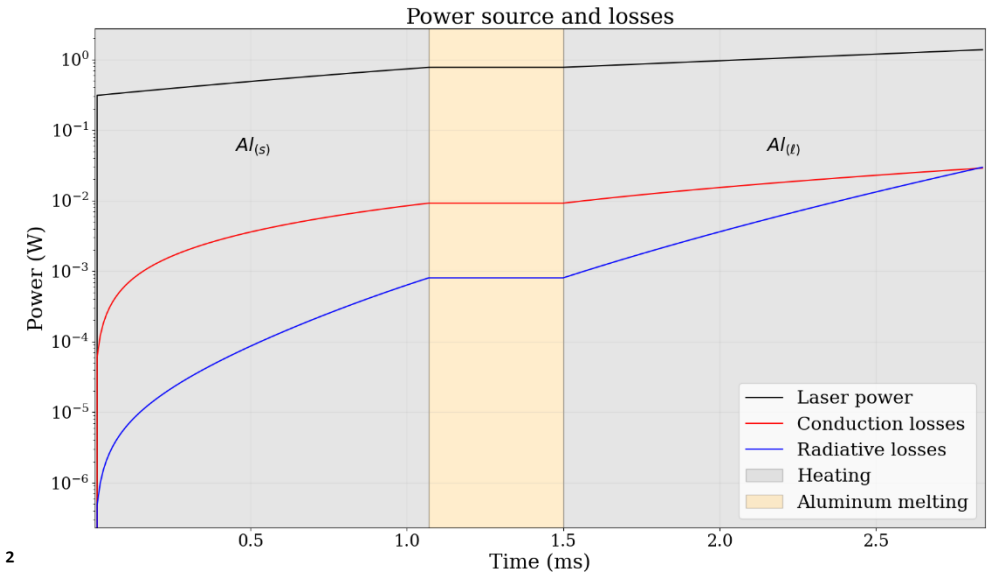

Figure 4 : Contribution of the different terms of the energy equation (Eq. 13) for an Aluminum particle of 88 µm in diameter heated by a CO_2 laser beam ($P_{LASER} = 42\ W$).

The measured and simulated temperature evolutions are shown in Figure 5. The raw (red solid line) and smoothed (black solid line) experimental traces are plotted with the modelled temperature evolution (dashed black line). The current system using photomultipliers is not sensitive enough to provide information on the evolution of the temperature below 1200 K. Aluminum melting can therefore not be detected. This particular point will be improved in the future.

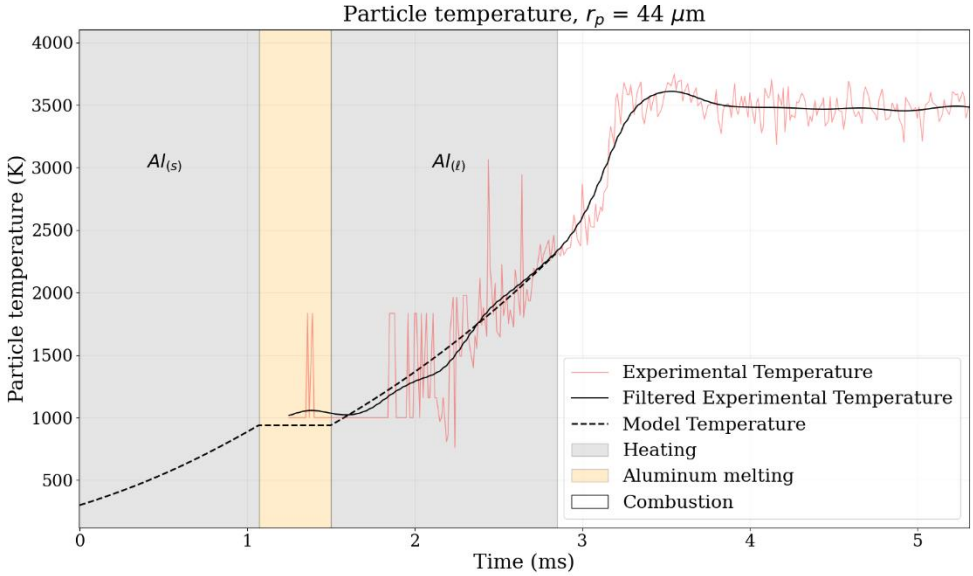

Figure 5 : Particle temperature evolution until ignition. Red solid line: raw experimental results; Black solid line: smoothed experimental results; Black dashed line: Model. Particle of aluminum in atmospheric air $(r_p = 88\ \mu m)$

Once the aluminum is liquified, the temperature of the particle increases rapidly up to about 2500 K (around 3 ms). During this phase, the absorption efficiency increases and therefore more laser power is transmitted to the particle. According to Figure 3, alumina melting and thermal runaway occur shortly after 3 ms, once the passive oxide layer melts. Is it observed in Figure 5 that this moment occurs around 2500 K, i.e., slightly above the alumina melting temperature. The difference between the measured temperature and the expected one may be due to a non-uniform heating on either side of the particle due to a slight asymmetry in the power distribution of the two laser beams. Under these conditions, one side may be slightly overheated before complete fusion of the oxide.

Once ignition starts, the gas phase combustion process takes place with a maximum surface temperature slightly below 3500 K, which agrees with thermodynamic calculations.

The proposed model accurately predicts the characteristic times for the different phases (i.e. solid and liquid aluminum heating and aluminum melting), which confirms the hypothesis that no exothermic surface reaction occurs before thermal runaway.

6. Conclusions

This study focuses specifically on the ignition of a micrometric aluminum particle stabilized in a levitator. The particle is heated up using a laser which gives access to heating rates of relevance for industrial systems (i.e., in the order of $10^6\ K/s$). To complete the detailed visualizations of the combustion process, a two-color pyrometry diagnostics has been set up which allows following the time evolution of the particle's temperature. The experimental results are compared with a simplified heating model. In particular, the different heating phases are very decently reproduced. Thermal runaway is triggered by the rupture of the oxide layer which occurs after melting. At this level of heating rate, the process is shown to be almost adiabatic as radiation and diffusion heat losses from the particle to the surroundings are almost negligible. Moreover, surface reactions do not have time to take place on the surface once the aluminum is in contact with the oxidizing atmosphere. Thermal runaway is almost immediate, occurring at time scale shorter than 50 microseconds after the heating started.

Acknowledgements

This work was supported by the region of « Centre Val de Loire » and the European Regional Development Funds (FEDER).

References

[1] Zhang S, Dreizin EL. Reaction Interface for Heterogeneous Oxidation of Aluminum Powders. The Journal of Physical Chemistry C. 2013;117:14025-31. 10.1021/jp402990v.

[2] Sundaram DS, Yang V, Zarko VE. Combustion of nano aluminum particles (Review). Combustion, Explosion, and Shock Waves. 2015;51:173-96. 10.1134/s0010508215020045.

[3] Rufino B, Boulc'h F, Coulet MV, Lacroix G, Denoyel R. Influence of particles size on thermal properties of aluminium powder. Acta Mater. 2007;55:2815-27. 10.1016/j.actamat.2006.12.017.

[4] Jeurgens LPH, Slook WG, Tichelaar FD, Mittemeijer EJ. Growth kinetics and mechanisms of aluminum-oxide films formed by thermal oxidation of aluminum. J Appl Phys. 2002;92:1649-56. 10.1063/1.1491591.

[5] Friedman R, Maček A. Combustion studies of single aluminum particles. Symposium (International) on Combustion. 1963;9:703-12. https://doi.org/10.1016/S0082-0784(63)80078-8.

[6] Merzhanov A, Grigorjev YM, Gal'chenko YA. Aluminium ignition. Combust Flame. 1977;29:1-14.
[7] Bazyn T, Krier H, Glumac N. Combustion of nanoaluminum at elevated pressure and temperature behind reflected shock waves. Combust Flame. 2006.
[8] Mohan S, Dreizin EL. Aluminum particle ignition in mixed environments. 47th AIAA Aerospace Sciences Meeting including the New Horizons Forum and Aerospace Exposition2009.
[9] Bar-Ziv E, Sarofim AF. The electrodynamic chamber: A tool for studying high temperature kinetics involving liquid and solid particles. Prog Energy Combust Sci. 1991;17:1-65. https://doi.org/10.1016/0360-1285(91)90002-5.
[10] Panagiotou T, Levendis YA, Delichatsios M. Measurements of Particle Flame Temperatures Using Three-Color Optical Pyrometry. Combust Flame. 1996;104:272-87.
[11] Monier R, Thumerel F, Chapuis J, Soulié F, Bordreuil C. Liquid metals surface temperature fields measurements with a two-colour pyrometer. Measurement. 2017;101:72-80. 10.1016/j.measurement.2016.12.031.
[12] Levendis YA, Estrada KR, Hottel HC. Development of multicolor pyrometers to monitor the transient response of burning carbonaceous particles. Rev Sci Instrum. 1992;63:3608-22. 10.1063/1.1143586.
[13] González de Arrieta I, Blanchard C, Laboureur P, Chauveau C, Genevois C, Rozenbaum O, et al. Radiative properties of micron-sized Al/air premixed flames described by an effective medium core-shell formulation. Int J Heat Mass Transfer. 2023;203. 10.1016/j.ijheatmasstransfer.2022.123815.
[14] Guibaud A, Citerne JM, Consalvi JL, Torero JL, Fujita O, Kikuchi M, et al. Accessing the soot-related radiative heat feedback in a flame spreading in microgravity: optical designs and associated limitations. Proc Combust Inst. 2021;38:4805-14. 10.1016/j.proci.2020.06.036.
[15] Guibaud A, Citerne JM, Orlac'h JM, Fujita O, Consalvi JL, Torero JL, et al. Broadband modulated absorption/emission technique to probe sooting flames: Implementation, validation, and limitations. Proc Combust Inst. 2019;37:3959-66. 10.1016/j.proci.2018.06.199.
[16] Braconnier A, Gallier S, Halter F, Chauveau C. Aluminum combustion in CO2-CO-N2 mixtures. Proc Combust Inst. 2021;38:4355-63. 10.1016/j.proci.2020.06.028.
[17] Mohan S. Experiment and modeling : ignition of aluminum particles with a CO2 laser. Dissertations. 2009;893.
[18] Qiu TQ, Longtin JP, Tien CL. Characteristics of Radiation Absorption in Metallic Particles. J Heat Transfer. 1995;117:340-5.
[19] Halter F, Glasziou V, Lorenzo MD, Gallier S, Chauveau C. Peculiarities of aluminum particle combustion in steam. Proc Combust Inst. 2022. 10.1016/j.proci.2022.07.120.
[20] Braconnier A, Chauveau C, Halter F, Gallier S. Experimental investigation of the aluminum combustion in different O2 oxidizing mixtures: Effect of the diluent gases. Exp Therm Fluid Sci. 2020;117. 10.1016/j.expthermflusci.2020.110110.